SAFETY STUDIES ON HYDROGEN PRODUCTION SYSTEM WITH A HIGH TEMPERATURE GAS-COOLED REACTOR

TETSUAKI TAKEDA
HTGR Performance and Safety Demonstration Group
Nuclear Applied Heat Technology Division
Nuclear Science and Engineering Directorate
Japan Atomic Energy Agency
Oarai-machi, Higashiibaraki-gun, Ibaraki-ken, 311-1393, JAPAN
E-mail : takeda.tetsuaki@jaea.go.jp

Received October 17, 2005

A primary-pipe rupture accident is one of the design-basis accidents of a High-Temperature Gas-cooled Reactor (HTGR). When the primary-pipe rupture accident occurs, air is expected to enter the reactor core from the breach and oxidize in-core graphite structures. This paper describes an experiment and analysis of the air ingress phenomena and the method for the prevention of air ingress into the reactor during the primary-pipe rupture accident. The numerical results are in good agreement with the experimental ones regarding the density of the gas mixture, the concentration of each gas species produced by the graphite oxidation reaction and the onset time of the natural circulation of air.

A hydrogen production system connected to the High-Temperature Engineering Test Reactor (HTTR) is being designed to be able to produce hydrogen by themo-chemical Iodine-Sulfur process, using a nuclear heat of 10 MW supplied by the HTTR. The HTTR hydrogen production system is first connected to a nuclear reactor in the world; hence a permeation test of hydrogen isotopes through heat exchanger is carried out to obtain detailed data for safety review and development of analytical codes. This paper also describes an overview of the hydrogen permeation test and permeability of hydrogen and deuterium of Hastelloy XR.

KEYWORDS : High-Temperature Gas-Cooled Reactor, Passive Safe Technology, Natural Circulation, Molecular Diffusion, Hydrogen Production System, Hydrogen Permeation, Hastelloy XR, Permeability

1. INTRODUCTION

The inherent properties of a High-Temperature Gas-cooled Reactor (HTGR) facilitate the design of the HTGR with high degree of passive safe performances, compared to other type of reactors. However, it is still not clear if the present HTTR (High-Temperature Engineering Test Reactor) [1] type reactor can maintain a passive safe function during the primary-pipe rupture accident, or what would be a design criterion to guarantee HTGR with the high degree of passive safe performances during the accident. The primary-pipe rupture accident is one of the most common of accidents related to the basic design regarding an HTGR, which has a potential to cause the destruction of the reactor core by oxidizing in-core graphite structures and to release fission products by oxidizing graphite fuel elements. It is a guillotine type rupture of the double coaxial pipe at the nozzle part connecting to the bottom of the reactor pressure vessel, which is a peculiar accident for the HTTR type reactor. When the primary-pipe rupture accident happens, one may assume that air entering into the reactor pressure vessel reacts with high temperature graphite structures and causes temperature rise of the reactor core and corrosion of the graphite components. Therefore, it is very important to make sure that the air ingress process during the primary-pipe rupture accident cannot seriously oxidize the graphite fuel elements to release the radioactive materials from the reactor core to the environment nor severely damage the graphite components to loose the integrity of the reactor internals. In order to predict or analyze the process of air ingress during the primary-pipe rupture accident of HTGRs, it is very important to develop computer programs and to validate them by experiments. This paper describes a computer program, which is named FLOWGR, developed to analyze the process of air ingress during the first stage of the primary-

pipe rupture accident in the case of the primary-pipe attached to the bottom part of the reactor core. An overview of the method is given for the prevention of air ingress into the reactor during the primary-pipe rupture accident. The numerical results are in good agreement with the experimental ones regarding the density of the gas mixture, the concentration of each gas species produced by the graphite oxidation reaction and the onset time of the natural circulation of air.

On the other hand, the research and development (R&D) program on nuclear production of hydrogen was started in January, 1997 as a study consigned by Ministry of Education, Culture, Sports, Science and Technology. After the reactor performance and safety demonstration test using the HTTR will be performed for several years, the hydrogen production system [2] will be connected with the HTTR. Prior to coupling of the hydrogen production system with the HTTR, the out-of-pile test [3], [4] and design study are performed to confirm the controllability, operability and safety of this system under simulated operational conditions and to establish the connection technology between the HTTR and the hydrogen production system. In order to obtain detailed data for a safety review and development of numerical analysis codes, an experiment on permeation of hydrogen isotope [5], a corrosion test of the reforming tube, and an integrity test of the high-temperature isolation valve [6] are being performed as an essential test in parallel to the out-of-pile test. The present paper also describes experimental results of hydrogen and deuterium permeability of Hastelloy-XR.

2. PREVENTION OF AIR INGRESS DURING THE PRIMARY-PIPE RUPTURE ACCIDENT

The full power operation (30 MW) of the HTTR, which is the first HTGR in Japan, was achieved in December 2001 at Japan Atomic Energy Agency (JAEA). It is a graphite-moderated high-temperature gas-cooled thermal reactor. A schematic drawing of the HTTR and the coolant

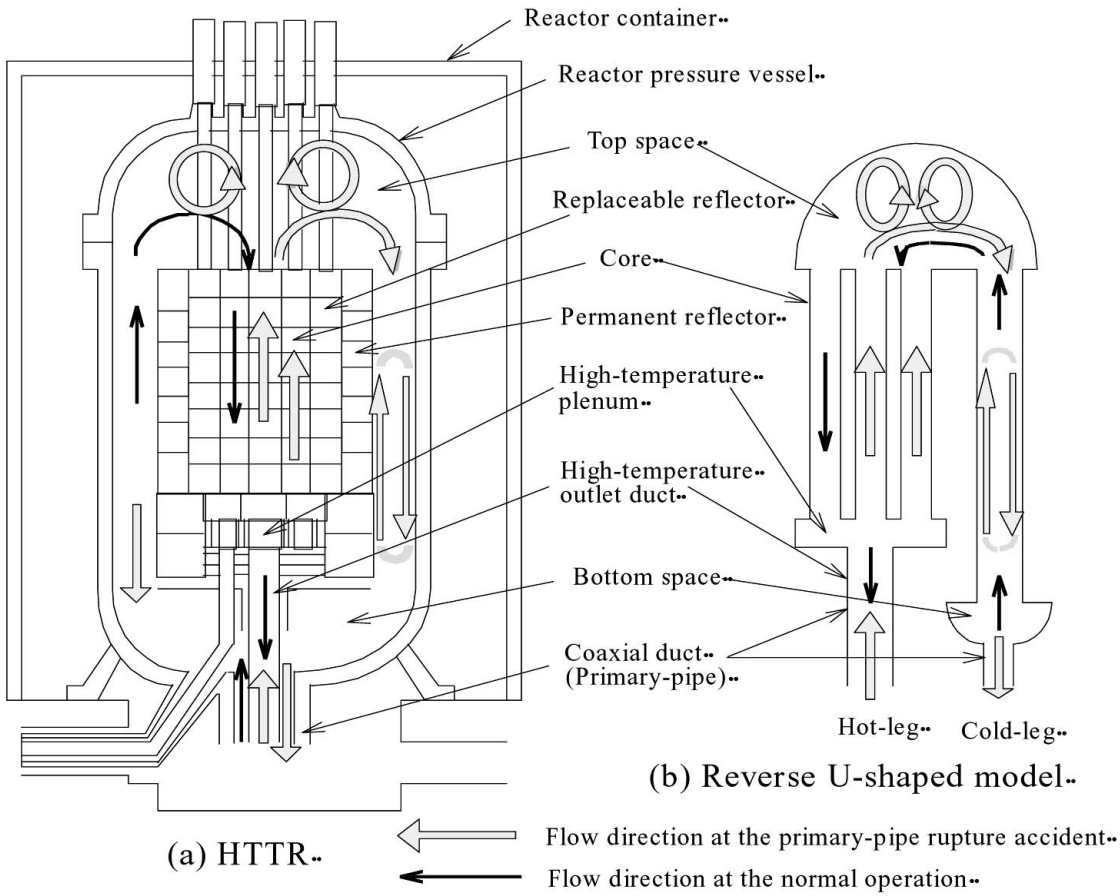

Fig. 1. Schematic Drawing of the HTTR and the Model of the Coolant Passages in the Reactor

passages in the reactor are provided in Fig. 1 (a). A hot leg consists of an inner passage of a coaxial duct, a high-temperature outlet duct, a high-temperature plenum and fuel cooling channels. A cold leg consists of an annular passage of the coaxial duct, a bottom cover and an annular passage between the reactor pressure vessel and permanent reflector. As the hot and cold legs are connected at the top space, they make a kind of reverse U-shaped tube as shown in Fig. 1 (b). When the primary-pipe rupture accident occurs, the high-pressure helium gas coolant in the reactor is forced out into the reactor containment through the breach. Gas pressure should become balanced between the inside and outside of the reactor pressure vessel. During this stage, called the depressurization stage, air is not able to enter the reactor core from the breach. After the depressurization stage, it is supposed that air enters the reactor core from the breach due to molecular diffusion and natural circulation of a multicomponent gas mixture induced by the distribution of gas temperature and the resulting concen-trations in the reactor. Carbon monoxide (CO) and dioxide (CO_2) are produced in the reactor, because the oxygen (O_2) contained in air reacts with the high temperature graphite structures. The density of the gas mixture in the reactor gradually increases as air enters by the molecular diffusion and natural circulation of the gas mixture in the first stage of the accident. Finally, the second stage of the accident starts after the natural circulation of air occurs suddenly throughout the entire reactor.

Previous studies focused mostly on molecular diffusion and natural circulation of the two-component gas mixture in a reverse U-shaped tube and in a simple test model of the HTTR [7]. In order to investigate the basic features of the flow behavior of the multicomponent gas mixture, consisting of helium (He), nitrogen (N_2), O_2, CO_2, CO, etc., experimental and numerical studies were performed on the combined phenomena of the molecular diffusion and the natural circulation of the multicomponent gas mixture with the graphite oxidation reaction in the reverse U-shaped tube [8]. The numerical results were in good agreement with the experimental ones regarding the density change of the gas mixture, the mole fraction change in the gas species and the onset time of the natural circulation of air. In order to understand the air ingress process in the HTTR and to validate the computer code, however, it is absolutely necessary to investigate the phenomena in a test facility that simulates the HTTR design. For these purposes, a test apparatus was constructed, which simulates the HTTR, and experiments simulating the primary-pipe rupture accident of the HTTR were carried out [9]. Based on the results of these fundamental studies, computer codes were developed to predict air ingress processes for various designs of the HTTR type reactor [10]. Furthermore, the

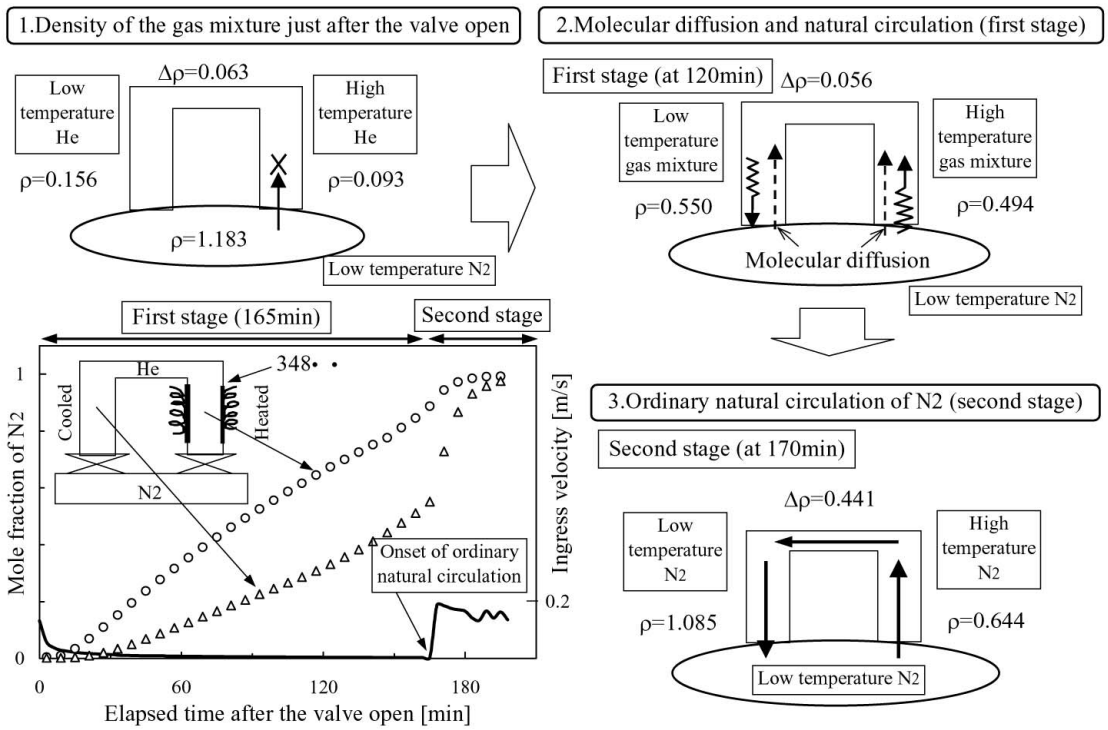

Fig. 2. Basic Feature of Nitrogen Ingress Process in a Reverse U-Shaped Tube

objectives of this study are to investigate the air ingress process and to develop the passive safe technology for the prevention of air ingress. This paper describes a computer program, which is named FLOWGR, developed to analyze the process of air ingress during the first stage of a primary-pipe rupture accident, and gives experimental results regarding the method for the prevention of air ingress into the reactor during the accident. The experimental results show that the helium injection process is a useful method for the prevention of air ingress [11] in the HTTR type reactor.

3. BASIC FEATURE OF AIR INGRESS PROCESS IN A REVERSE U-SHAPE TUBE

Experimental and numerical studies were performed on the combined phenomena of molecular diffusion and natural circulation in a two-component gas system (N_2-He) in a reverse U-shaped tube. Figure 2 shows an example of the mole fraction and the ingress velocity changes of N2 in the reverse U-shaped tube. The solid line in the figure is the ingress velocity obtained by the hot-wire anemometer attached at the lower end of the high-temperature side pipe. The symbols (o) and (Δ), respectively, represent the mole fraction changes at the same distance (600 mm) from the lower ends of the both side pipes. The mole fraction of N_2 at the high-temperature side pipe is higher than that at the low-temperature side pipe. This is because N_2 is transported upward by the molecular diffusion from the both ends of the pipes and by the natural circulation of the gas mixture having the very slow velocity from the high-temperature side to the low-temperature side pipe.

According to the results obtained, the density of the gas mixture in the reverse U-shaped tube gradually increases as N_2 enters as a result of molecular diffusion and because of a very weak natural circulation of the gas mixture. The calculated velocity of this very weak natural circulation of the gas mixture is about 10^{-6}~10^{-3}m/s (10^{-4}<Re<1). The ordinary natural circulation of N_2, which is about 0.2m/s (Re>200) in Fig.2, occurs suddenly throughout the reverse U-shaped tube, because the buoyancy force has risen to such an extent as to bring about the natural circulation. The time required from the first stage to the second stage is about 10 seconds in the ingress process. Therefore, the production process of the second stage is a rapid phenomenon because the duration time of the first stage is about 165 minutes in the reverse U-shaped tube.

4. EXPERIMENTAL APPARATUS

Figure 3 shows an experimental apparatus, which consists of a reactor core simulator, a high-temperature plenum, a water-cooled jacket corresponding to the reactor pressure vessel and simulated inlet and outlet pipes corresponding to the coaxial tube. The reactor core simulator has 4 graphite pipes, a ceramic plenum, and electric heaters. The graphite pipe has an inner diameter of 40mm and a length of 800mm. The reactor core simulator divides into 12 temperature regions, which is the upper, middle, and lower part of each graphite pipe. The graphite pipe temperature in each region can automatically be controlled individually. The inlet pipe simulates the outer pipe of the double coaxial primary-pipe of the HTTR. It has an inner diameter of 69.3mm. The outlet pipe simulates the inner pipe of the high-temperature primary-pipe. An upper part of the outlet pipe is made of ceramic and a rest lower part is made of stainless steel. The inner diameter of the outlet pipe is 69.3mm. At the bottom ends of the outlet and inlet pipe, ball valves are equipped to simulate the primary-pipe rupture accident. The pressure vessel simulates the reactor pressure vessel of the HTTR and it has a height of 2003mm and an inside diameter of 920mm. A partition plate is installed in the top space of the pressure vessel to lessen the volume of the top space, which shortens experiment time required for one run. The annular passage between the inner barrel and the pressure vessel has a gap of 60mm. The main specifications of the experimental apparatus are provided in Table 1. To measure the ingress velocity of air, an ultra sonic anemometer is equipped with the lower end of the outlet pipe. The temperatures of the gas mixture, the reactor core simulator and other structures were continuously measured at the inlet and outlet pipes, the high-temperature plenum, the top space and the annular passage between the inner barrel and the pressure vessel as shown in Fig.3. The gas mixture in the apparatus was sampled at five positions as indicated in Fig.3. The density of the gas mixture, the mole fraction of O_2, CO_2 and CO was measured using a gas analyzer.

5. CORE COOLING EXPERIMENT

In order to investigate the safe cooling rates of the reactor core during the accident, we carried out the core cooling experiment using the test apparatus. Figure 4 shows the analytical results of the maximum temperature in the fuel block, the upper and lower replaceable reflector block during the accident at the end of core life of the HTTR [12, 13]. The maximum temperature in the fuel blocks decreases rapidly after the reactor scram and then increases slightly due to decay heat. The peak fuel temperature is 1380ºC at about 30 hours after the accident was happened. The temperature of the fuel block is lower than 750ºC at 330 hours and that of the replaceable reflectors are lower than 750ºC at about 50 hours after the accident were started.

Figure 5 shows the average temperature change of the graphite pipe with kept at constant temperature after the simulated pipe rupture. In the case of the average temperature of the graphite pipe exceeds 750ºC, the temperature of the graphite pipe increases after the second stage of

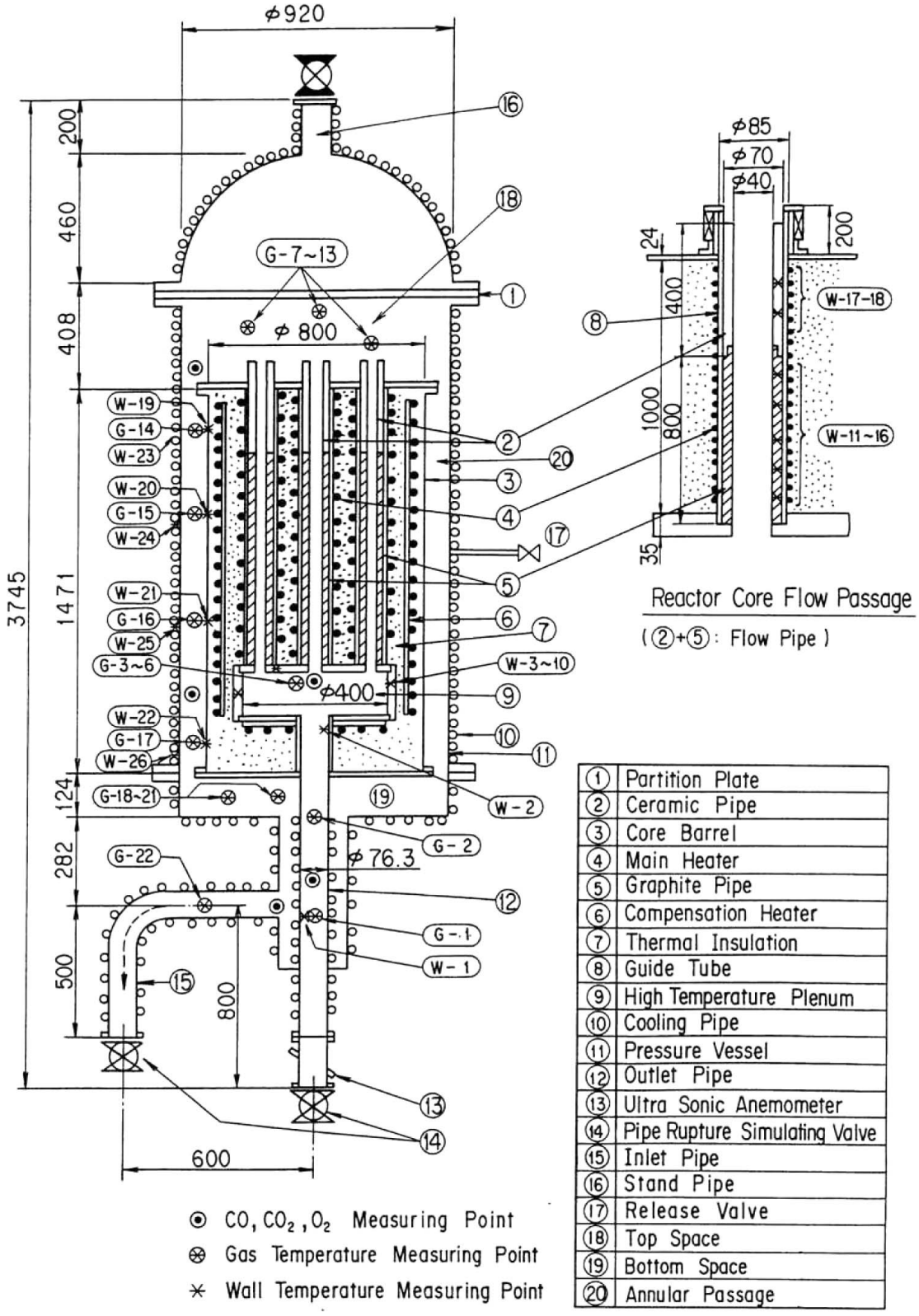

Fig. 3. Experimental Apparatus

Table 1. Main Specifications of Experimental Apparatus

Pressure:	~0.27 MPa
Temperature:	~1,200℃
Dimension and material:	
Reactor core flow passage:	
Graphite pipe	IG-110 (Toyo Tanso), 40mm ϕ I.D. ×70mm ϕ O.D. ×800mm
Ceramic pipe	Al_2O_3 (Kyocera), 40mm ϕ I.D. ×70mm ϕ O.D. ×400mm
Guide pipe	Al_2O_3 (Kyocera), 73mm ϕ I.D. ×85mm ϕ O.D. ×1,250mm
High-temperature plenum:	Al_2O_3 (Kyocera), 400mm ϕ I.D. ×460mm ϕ O.D. ×150mm
Core barrel (inner barrel):	Stainless steel, 800mm ϕ ×1,519mm
Top cover:	Carbon steel, 460mm in radius
Pressure vessel:	Carbon steel, 920mm ϕ I.D.
Outlet pipe:	Al_2O_3 (Kyocera), 69.3mm ϕ I.D. × 80mm ϕ O.D. ×315mm
	Stainless steel, 69.3mm ϕ I.D. ×76.3mm ϕ O.D. ×800mm
	Carbon steel, 69.3mm ϕ I.D. ×76.3mm ϕ O.D. ×260mm (Ultra sonic anemometer)
Inlet pipe:	Stainless steel, 69.3mm ϕ I.D. ×76.3mm ϕ O.D. ×1,100mm
Total height of test apparatus:	3,750mm

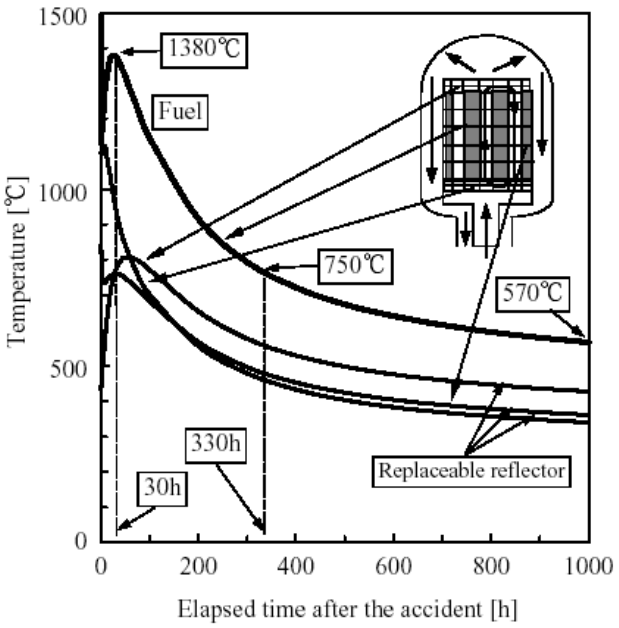

Fig. 4. Analytical Results of the Fuel Block Temperature Change During the Accident

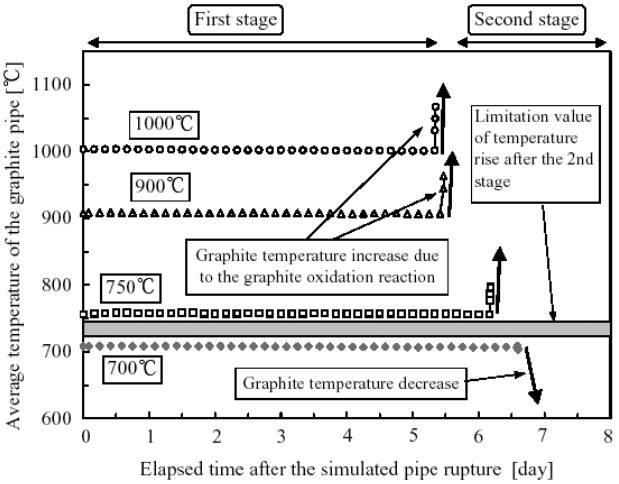

Fig. 5. Average Temperature Change of the Graphite Pipe with Kept at Constant Temperature

the accident due to the graphite oxidation reaction. On the other hands, in the case of the temperature lower than 700ºC, the temperature of the graphite pipe decreases after the onset of the ordinary natural circulation of air. This is because the natural circulation of cold air cools the simulated core and the reaction rate of the graphite oxidation becomes slow. Thus, it is supposed that the limitation value of temperature rise after the second stage exists between 700ºC and 750ºC in the graphite temperature.

Figure 6 shows the average temperature change of the graphite pipe when the simulated core is cooled by means of the various cooling rates after the simulated pipe rupture. The cooling rate of the graphite pipe is defined by the duration time of the first stage in the case of 1000ºC experiment. The duration time of the first stage is about 128 hours in the case of the constant temperature experiment kept at 1000ºC. Hence, if the temperature of the graphite pipe decreases from 1000ºC to 20ºC during 128 hours, the cooling rate of the graphite pipe is about 7.7ºC/h. This cooling rate determined as the standard rate. In Fig.6, exp. (1) means the constant temperature experiment kept at

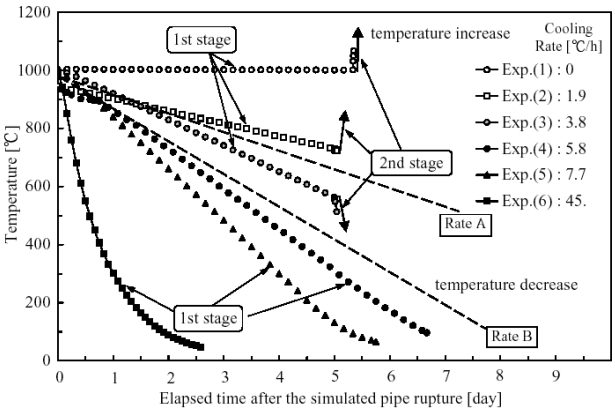

Fig. 6. Average Temperature Change of the Graphite Pipe in the Core Cooling Experiment

1000ºC, and exp. (2), (3), (4) and (5) defined as the case of 1/4, 1/2, 3/4 and 1 of the standard rate, respectively. Exp. (6) defined as the case of all electric heater power shut down. When the cooling rate ranges from 0ºC/h to 1.9ºC/h (exp. (1) and (2)), the ordinary natural circulation of air produces at about 5 days later and then the temperature of the graphite pipe increases due to the graphite oxidation reaction. In the case of the cooling rate is 3.8ºC/h (exp. (3)), the duration time of the first stage is almost same as the case when the rate is lower than 1.9ºC/h. However, the temperature of the graphite pipe decreases in the second stage because the reaction rate becomes slow. Further more, when the cooling rate is higher than 5.8ºC/h (exp. (4), (5) and (6)), the second stage cannot establish and the air ingress process terminates during the first stage. Therefore, two kinds of the safe cooling rate (Rate A and B) exist in this experiment. On these results, it is supposed that the safe cooling rate of the HTTR during the accident also exists.

6. NUMERICAL ANALYSIS

6.1 Features of the Program

FLOWGR provides a numerical method for analyzing the transient thermal hydraulic behavior by solving the one-dimensional basic equations for continuity, momentum conservation, energy conservation of the gas mixture, and the mass conservation of each gas species. The main features of FLOWGR are explained in the following:

(1) FLOWGR treats the gas mixture consisting of arbitrary components and takes into account the graphite oxidation and CO combustion reactions. The source and sink terms in the mass conservation equations resulting from these chemical reactions are expressed by the temperature dependent Arrhenius formula having rate constants, which are specified by the user.

(2) The reactor system to be analyzed by FLOWGR is modeled as a network of one-dimensional stream-tubes, which represent components of the system such as a piping, plenum and reactor core. Each stream-tube is further divided into fluid volumes (control volumes or cells). There are three types of tube-ends: normal, break and closed end. The normal end connects with adjacent stream-tubes, the closed end has no adjacent stream-tube and the break end represents the breach connected to the open air.

6.2 Basic Equations

The basic equations (mass-based formulation) are as follows.

The equation of continuity for the gas mixture:

$$\frac{\partial \rho}{\partial t}+\frac{\partial(\rho u)}{\partial x}=\sum_{i=1}^{n} Q_i \,. \tag{1}$$

The equation of mass conservation for each gas species:

$$\frac{\partial(\rho \omega_i)}{\partial t}+\frac{\partial(\rho u \omega_i)}{\partial x}=\frac{\partial}{\partial x}\left(\rho D_{i-m}\frac{\partial \omega_i}{\partial x}\right)+Q_i \,, \tag{2}$$

for i=1 to n-1, and $\omega_n = 1-\sum_{k=1}^{n-1}\omega_k$.

The equation of energy conservation:

$$\frac{\partial(\rho c_p T)}{\partial t}+\frac{\partial(\rho u c_p T)}{\partial x}=\frac{\partial}{\partial x}\left(\lambda\frac{\partial T}{\partial x}\right)+\alpha\frac{L_h}{A_e}(T_w-T). \tag{3}$$

The equation of momentum conservation:

$$\frac{\partial(\rho u)}{\partial t}+\frac{\partial(\rho u^2)}{\partial x}=-\frac{\partial p}{\partial x}-\rho g\cos\theta-\frac{1}{2}\rho u|u|\left(\frac{f}{D_e}\right). \tag{4}$$

The equation of state for the gas:

$$pM_m=\rho RT \quad \text{or} \quad p=CRT \,. \tag{5}$$

Here, the friction factor (f) and the heat transfer coefficient (α) corresponding to the fully developed laminar flow are used [14]. The viscosity (μ) and thermal conductivity (λ) of each gas species and the gas mixture is obtained using the Wilke method and by the Eucken correlation [15], respectively.

The other set of the basic equations (molecule-based formulation) includes the equations of continuity (Eq.(6)) and of number of molecules conservation for each gas species (Eq.(7)) instead of Eq.(1) and Eq.(2).

The equation of continuity for the gas mixture:

$$\frac{\partial C}{\partial t}+\frac{\partial(Cu)}{\partial x}=\sum_{i=1}^{n}\left(Q_i \big/ M_i\right). \tag{6}$$

The equation of number of molecules conservation for each gas species:

$$\frac{\partial(CX_i)}{\partial t}+\frac{\partial(CuX_i)}{\partial x}=\frac{\partial}{\partial x}\left(CD_{i-m}\frac{\partial X_i}{\partial x}\right)+Q_i/M_i . \quad (7)$$

For i=1 to n-1, and $X_n = 1-\sum_{k=1}^{n-1} X_k$.

Where X_i = mole fraction for the component gas i, M_i = molecular weight. In this set of equations, the conservation equation of momentum (Eq.(4)) and the equation of state for the gas (Eq.(5)) are used. However, the equation of energy conservation (Eq.(3)) is omitted based on the assumption that the gas temperature is equal to the wall temperature.

The diffusion coefficients D_{i-m} for the multi-component gas system are obtained from the diffusion coefficients for the binary gas system and the mole fractions of each gas species.

$$D_{i-m}=\frac{1-X_i}{\sum_{j=1}^{n}\frac{X_j}{D_{i-j}}} \quad (8)$$

This coefficient is called the effective diffusion coefficient in the multi-component gas mixture, which is provided by references [16], [17], [18].

In the present analysis, the graphite oxidation reaction (C-O_2 reaction) and the carbon monoxide combustion (CO-O_2 reaction) are taken into account. The dissipation or generation terms Q_i of the mass conservation equations for O_2, CO and CO_2 are written as:

$$Q_i = Q_i^{(1)} + Q_i^{(2)}, \quad (9)$$

Where $Q_i^{(1)}$ is the term for the graphite oxidation reaction and $Q_i^{(2)}$ the one for the CO combustion. Using the arrhenius formula, these terms are

$$Q_i^{(1)} = K_i^{(1)} \exp\left(-\frac{E_1}{RT}\right), \quad (10)$$

$$Q_i^{(2)} = K_i^{(2)} \exp\left(-\frac{E_2}{RT}\right). \quad (11)$$

Where $K_i^{(1)}$ and $K_i^{(2)}$ are constants, E_1 and E_2 the activation energies. Details of these constants and activation energies are explained in reference [8].

6.3 Numerical methods

The numerical methods are based on replacing the system of differential equations with a system of finite-difference equations fully implicit in time except the convection term for the momentum equation, which is treated explicitly. These results in a set of discretized nonlinear equations are solved by iteration procedure. In each iteration time, the implicit terms are formulated to be linear in the dependent variables at new time. The resulting linear systems are solved by direct inversion or a Gauss-Seidel iteration.

The finite-difference equations used in FLOWGR can be obtained by integrating the conservation equations over a fixed fluid volume. The scalar properties (pressure, temperature, etc.) of the flow are defined at the volume centers, while vector quantity (velocity) is defined at the junctions. The equations of continuity and mass conservation (Eqs.(1) and (2)), and the equation of energy conservation (Eq.(3)) for the mass-based formulation as well as the equations (Eqs.(6) and (7)) for the molar-based formulation are integrated with respect to the spatial variable x from the junction at x_j to the junction at x_{j+1}. The equation of momentum conservation (Eq.(4)) is integrated with respect to the spatial variable from the volume center at $x_{j+1/2}$ to the adjacent volume center at $x_{j+3/2}$. In this integration loss of pressure is taken into account at the volume boundary with abrupt area change. The fluxes due to convection and diffusion, which appear in the integrated equations, are approximated using the hybrid difference scheme [19], [20].

The finite-difference equations can be solved under the initial and boundary conditions. The initial conditions for the temperature, pressure and mole fractions for each component gas are specified at the volume centers and those for velocities at the junctions. In order to analyze the phenomenon just after the depressurization stage, it is assumed that the gas velocities are zero for the initial condition. As for the boundary conditions, the pressure, temperature, mole fractions of each gas species are specified at the end of the stream-tube, which has the break end. The wall temperature of the stream tubes is also specified for each control volume as a function of time. At the closed ends of the stream-tubes, the boundary conditions are that the flow velocity and fluxes due to convection and diffusion are zero.

In order to obtain stable and fast convergence of the nonlinear equations, the equations of continuity and of momentum conservation for the gas mixture linearized by the pressure and velocity are solved using the SIMPLER method proposed by Patankar [19] along with the other conservation equations linearized by the mass (mole) fractions and temperature. In this iteration procedure, the numerical relaxation is applied for the production and dissipation terms as well as for the dependent variables in such a way.

$$\Gamma_{new} = \delta\Gamma_{cal} + (1-\delta)\Gamma_{old} \quad (12)$$

Where Γ_{new} is a new value, Γ_{cal} a calculated value without the relaxation, Γ_{old} an old value and δ is a relaxation parameter, the value of which is chosen in a range $0< \delta <1$.

7. COMPARISON WITH EXPERIMENTS

The density and mole fraction changes in the apparatus were analyzed using FLOWGR. The apparatus is modeled

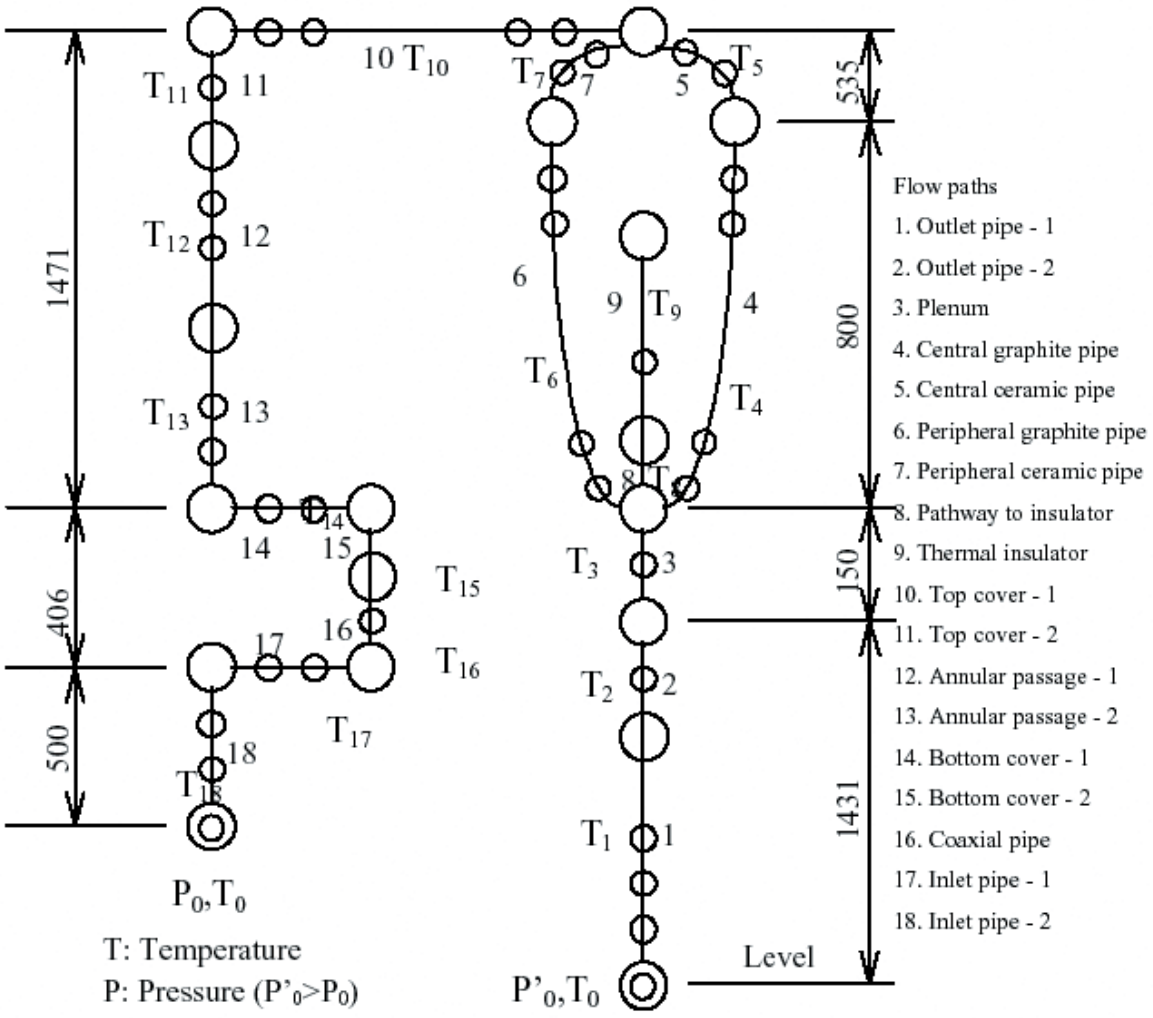

Fig. 7. Network Model of the Experimental Apparatus

as a network consisting of one-dimensional stream-tubes. Figure 7 shows the network model of the apparatus. At the beginning of the experiment, the apparatus was filled with helium gas. When the temperature of the gas and the reactor core simulator reached a steady state, the valves located at the ends of the inlet and outlet pipe were opened at the same time to simulate the pipe rupture accident condition.

The parameters of the stream-tubes are listed in Table 2. In this analysis, the molar-based formulation was used instead of the mass-based formulation. In the preliminary calculations, the two sets of formulations were checked by calculating the process of air ingress in a reverse-U-shaped tube with the graphite oxidation reaction. It has been found that fairly good agreements are obtained between the calculated results of the two sets of formulations with respect to the concentration changes of each gas species and the onset time of the natural circulation of air. It has also been found that the computations by the mass-based formulation take two to three times as much time as those by the molar-based formulation. In the case of a reverse-U-shaped tube model, the matrix structure of the simultaneous linear systems is the simple tri-diagonal type. Thus, the linear systems are efficiently solved by direct inversion. For the model which has a complex network with many stream branches as shown in Fig. 7, the discretized equations are expressed by sparse matrices having a large bandwidth. As it is expected much more computation time will be required, the molecule-based formulation was adopted and the Gauss-Seidel iteration method was used for this analysis.

Figures 8, 9, 10 and 11 show an example of the measured density and mole fraction changes of O_2, CO_2 and CO

at various measuring points. The average temperature of the reactor core simulator is about 900°C. The mole fractions of CO and CO_2 in the plenum and the top cover gradually increase by molecular diffusion and the very weak natural circulation until the onset of the natural circulation of air. The first stage of the accident lasted for about 5 days in the experimental apparatus which simulates the HTTR. From this study, it became clear that air ingress process is completely different in the first and second stages. The important mechanisms of the air ingress in the first stage of the accident are molecular diffusion and the very weak natural circulation of the gas mixture. It also became clear that the duration of the first stage period is fairly long.

The numerical results compared with the experimental ones are also shown in Figs. 8, 9, 10 and 11. As can been seen from these figures, the onset time of the natural circulation of air is fairly well reproduced and considerable agreements between the experiment and calculation are obtained for the density of the gas mixture and the mole

Table 2. Parameters of Stream-Tubes

Path number	Path name	Length (m)	Equiv. Diameter (m)	Wall temp. (°C)	C/O2 reaction	CO/O2 reaction	Vertical angle (deg.)
1	Outlet pipe – 1	1.15	0.0693	14-28	×	×	0
2	Outlet pipe – 2	0.47	0.0693	28-700	×	O	0
3	Plenum	0.17	0.3767	700-900	×	O	0
4	Central graphite pipe	0.8	0.04	908-908	O	O	0
5	Central ceramic pipe	0.5	0.0484	900-200	×	×	0
6	Peripheral graphite pipe	0.8	0.0693	908-908	O	O	0
7	Peripheral ceramic pipe	0.5	0.0838	900-200	×	×	0
8	Pathway to insulator	0.03	0.0417	900-900	×	×	0
9	Thermal insulator	1.4	0.7671	900-900	×	×	0
10	Top cover – 1	0.29	0.5919	104-104	×	×	90
11	Top cover – 2	0.2	0.8697	104-225	×	×	180
12	Annular passage – 1	0.76	0.4543	225-129	×	×	180
13	Annular passage – 2	0.76	0.4543	129-33	×	×	180
14	Bottom cover – 1	0.24	0.5155	29-29	×	×	90
15	Bottom cover – 2	0.15	0.3132	29-14	×	×	180
16	Coaxial pipe	0.23	0.2086	14-14	×	×	180
17	Inlet pipe – 1	0.5	0.0693	14-14	×	×	90
18	Inlet pipe – 2	0.5	0.0693	14-14	×	×	180

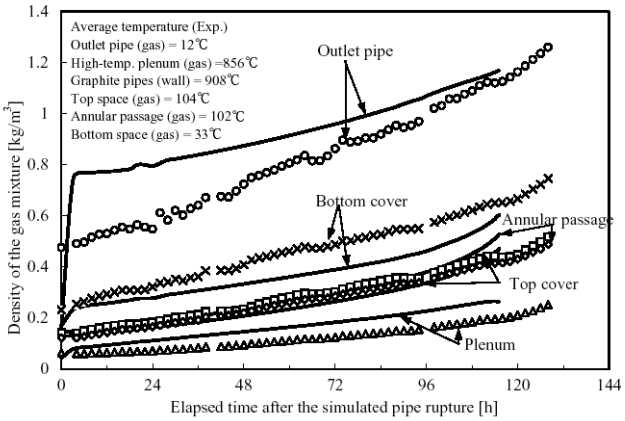

Fig. 8. Time Dependent Behavior of the Gas Mixture Density

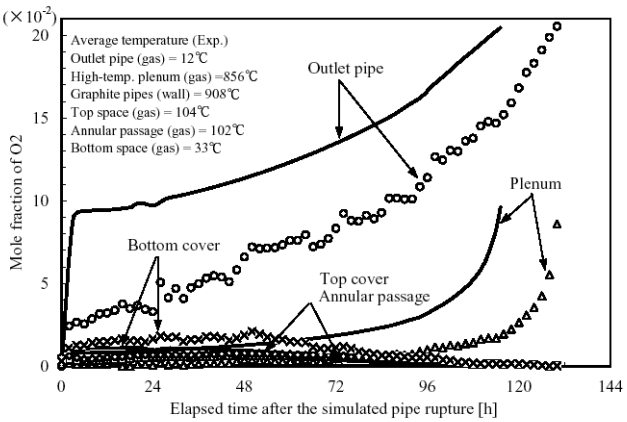

Fig. 9. Time Dependent Behavior of the Mole Fraction of Oxygen

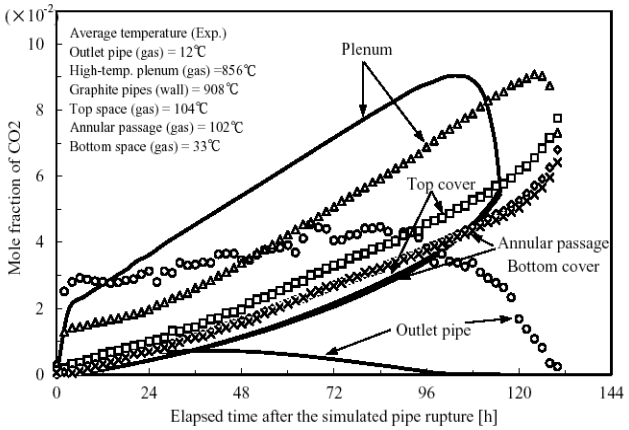

Fig. 10. Time Dependent Behavior of the Mole Fraction of Carbon Dioxide

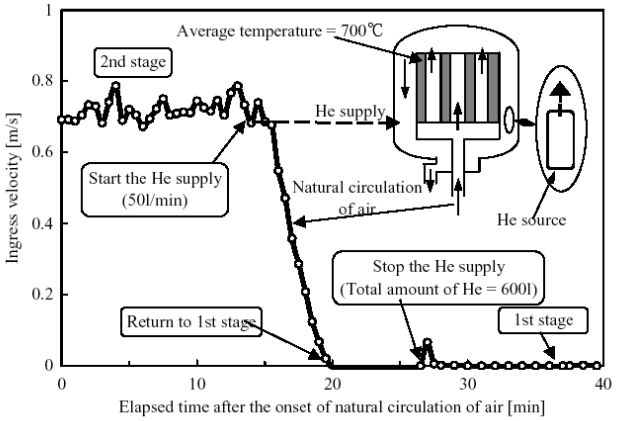

Fig. 12. Air Ingress Velocity Change During the Helium Injection Process

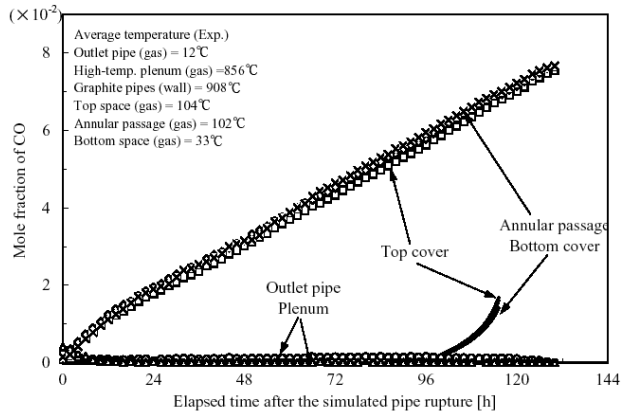

Fig. 11. Time Dependent Behavior of the Mole Fraction of Carbon Monoxide

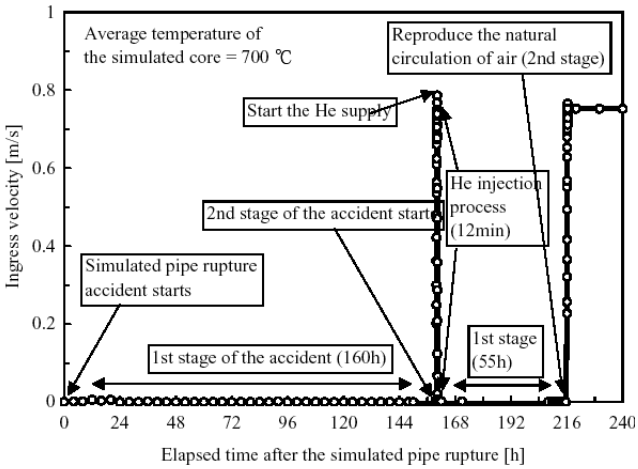

Fig. 13. Air Ingress Velocity Change During the Experiment

fractions of each gas species.

8. PASSIVE SAFE TECHNOLOGY EXPERIMENT

In order to develop the passive safe technology for the prevention of air ingress, the helium injection experiment has been carried out. The natural circulation of air induced by the density difference between two vertical legs in the reverse U-shaped tube can be controlled by the method of helium injection. That is, the buoyancy force due to the density difference as resulting the temperature difference between two vertical legs will be disappeared to inject helium which is lighter gas than air into the low-temperature leg filled with heavier gas. Thus, experimental procedures were as follows.

At first, the apparatus was filled with helium and the simulated core was heated up to 700ºC. The temperature in the apparatus was held constant during the first stage. The experiment started by opening the simulated pipe rupture valves attached to the inlet and outlet pipes at the same time. After the natural circulation of air began, helium gas was injected into the annular passage from the valve attached to the lower position of the pressure vessel. The amount of supplied helium was about 600 *l*, which is the same amount of the volume of the apparatus. The speed and the duration time of injection were 50 *l*/min and 12 minutes, respectively. In this experiment, an active method was used for the injection of helium gas. However, if the helium canister with small opening or crack can be installed into the lower part of the annular passage, the first stage can be maintained after the depressurization stage until the gas pressure in the canister decrease to the one in the annular passage.

Figure 12 shows an air ingress velocity change at the outlet pipe during the helium injection process. As indicated

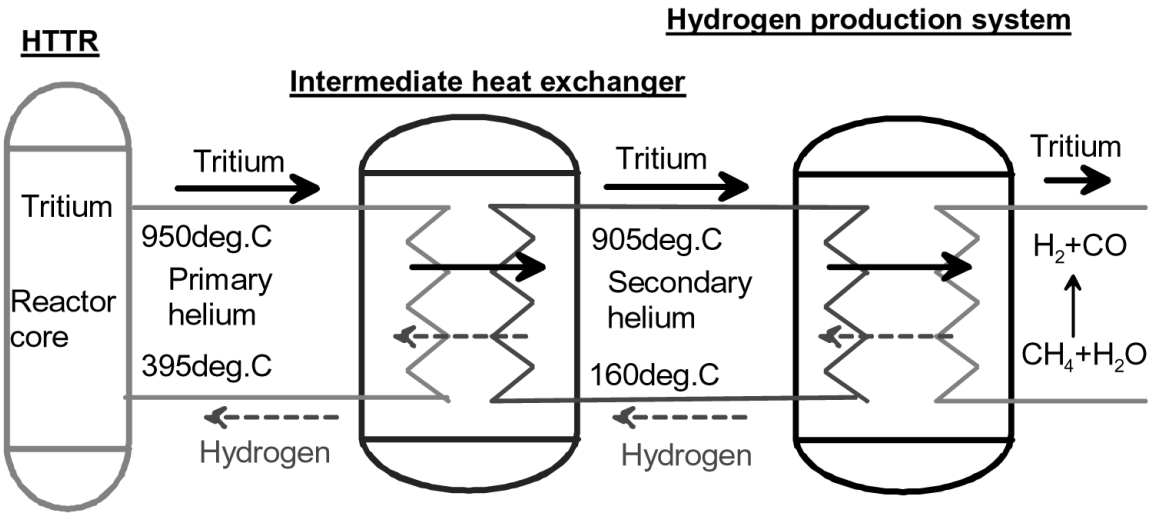

Fig. 14. Tritium and Hydrogen Transport Process in the HTTR Hydrogen Production System

in Fig. 12, the air ingress velocity became 0 during 5 minutes in the helium injection process. Thus, the air ingress process changed from the second stage to the first stage of the accident. After the helium injection process terminated, the experiment was carried out until the second stage restarted. Figure 13 shows the ingress velocity change of air during the present experiment. The duration time of the first stage of this experiment was about 160 hours. The ingress velocity during the second stage was about 80 cm/s. In the present experiment, the first stage continued again after the helium injection process terminated and the second duration time of the first stage was 55 hours. Finally, the natural circulation of air reproduced and the second stage of the accident restarted.

9. PERMEABILITY OF HYDROGEN AND DEUTERIUM IN THE HTTR HYDROGEN PRODUCTION SYSTEM

Permeation of tritium is an important problem in regard to a release of the radioactive substance from the HTTR hydrogen production system. Figure 14 shows an outline of tritium and hydrogen transport process when the conventional steam reforming hydrogen production system connects with the HTTR. There are several sources for a production of tritium in the HTTR [21]. In comparison to the other nuclear reactors, the HTTR has graphite components containing lithium as impurity in the reactor and its coolant gas helium has He-3 isotope, which produces tritium. The inventories of these sources have their maximum in the initial period of reactor operation and consequently due to burning up the amount of these nucleate decreases during reactor operation. Further sources are boron in the control rods and uranium in the fuel particles. Tritium, which produced in the reactor, permeates a heat transfer pipe of an intermediate heat exchanger (IHX) and transfers from a primary cooling system to a secondary cooling system. Finally, it seems to be probable that tritium permeates through the hydrogen production system and mixes in hydrogen as a product.

On the other hand, hydrogen produced in the application system and the heat transfer pipe of the IHX in opposite direction to permeation of tritium. Therefore, it is expected that hydrogen transfers to the primary cooling system and mixes in the helium gas coolant. As hydrogen gets into in the reactor core, a reduction of purification ability will take place due to rise in the concentration of impurities in the primary cooling system caused by the reaction of the graphite and hydrogen. The primary helium purification system of the HTTR is designed to have hydrogen concentration limited to less than 3 ppm. In order to connect the hydrogen production system with the HTTR, it is necessary to evaluate quantitatively the amount of permeated hydrogen through the IHX. Hastelloy XR, which is Nickel-based alloy, is used as a material of the heat transfer pipe of the IHX, because it is only approved as a high-temperature structural material under a high-pressure helium gas condition of the HTTR. In order to take the safety review of the HTTR hydrogen production system, it is necessary to evaluate not only the amount of permeated hydrogen isotope through the IHX but also the amount of tritium mixing in product hydrogen quantitatively. Therefore, it is necessary to obtain permeability of hydrogen isotope through Hastelloy XR tube prior to the construction of the HTTR hydrogen production system.

The aims of the hydrogen permeation test are, (i) to obtain the data of permeability of Hastelloy XR, (ii) to evaluate the effect of counter permeation of hydrogen isotopes, and (iii) to evaluate the effect of permeation

Table 3. Permeability of Hydrogen and Deuterium of High-Temperature Alloys

No.	High-temperature alloy	Pre-exponential factor K_0 [$m^3(STP) \cdot m^{-1} \cdot s^1 \cdot Pa^{-0.5}$]	Activation energy E_0 [$kJ \cdot mol^{-1}$]	Temperature T [℃]	Reference
1	Nickel	7.73×10^{-9}	54.84	-	Robertson, 1972[29]
2	Inconel-600	2.22×10^{-8}	66.14	800-1000	Masui et al., 1979[27]
3	Incoloy-600	1.00×10^{-8}	64.05	700-950	Mori & Nakada*, 1974[26]
4	Incoloy-800	2.13×10^{-8}	69.07	800-1000	Masui et al., 1979[27]
5	Incoloy-800	5.45×10^{-9}	64.05	700-950	Mori & Nakada*,1974[26]
6	Incoloy-800	2.31×10^{-8}	74.1	600-950	Rohrig et al., 1975[25]
7	Incoloy-800	9.77×10^{-9}	74.1	649	Strehlow & Savage**,1974[24]
8	Hastelloy-N	2.59×10^{-8}	77.99	605	Strehlow & Savage**,1974[24]
9	Hastelloy-X	5.62×10^{-9}	58.2	400-600	Namba et al., 1978[28]
10	Hastelloy-X	2.00×10^{-8}	66.98	800-1000	Masui et al., 1979[27]

* Some oxide film influence suspected.
** For deuterium

Table 4. Specifications for Chemical Compositions of Hastelloy XR and X [30]

Material	Range	Chemical compositions (wt%)														
		Elements														
		C	Mn	Si	P	S	Cr	Co	Mo	W	Fe	Ni	B	Al	Ti	Cu
Hastelloy XR	Max.	0.15	1.0	0.5	0.04	0.03	23.0	2.5	10.0	1.0	20.0	Remainder	.01	.05	.03	0.5
	Min.	0.05	0.75	0.25	-	-	20.5	-	8.0	0.20	17.0	Remainder	-	-	-	-
Hastelloy X	Max.	0.15	1.0	1.0	0.04	0.03	23.0	2.5	10.0	1.0	20.0	Remainder	.01	0.5	0.15	0.5
	Min.	0.05	-	-	-	-	20.5	0.5	8.0	0.20	17.0	Remainder	-	-	-	-

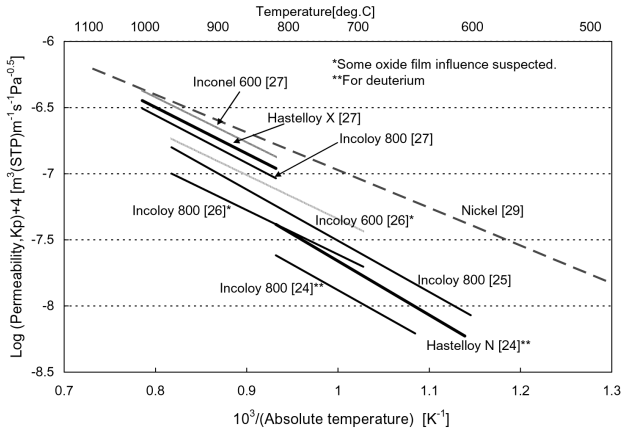

Fig. 15. Permeability of Hydrogen and Deuterium of High-Temperature Alloys

protection by oxide film [22], [23]. The basic data on the permeability of hydrogen and deuterium has been obtained for the Hastelloy XR tube in this test.

9.1 Permeation Test of Hydrogen Isotopes

9.1.1 Outline of the Test

A pre-exponential factor and activation energy of permeability of hydrogen and deuterium collected in Arrhenius type are provided in Table 3 and in Fig. 15. There are several reports of permeability of hydrogen and deuterium of a high-temperature alloy such as Incolloy [24], [25], [26], [27] and Hastelloy [24], [27], [28]. Hydrogen permeability of HK40, Incolloy 800, Hastelloy X and Inconel 600 in 800ºC-1000ºC was obtained by Masui et al. [27]. They reported that hydrogen permeability of these alloys approaches to that of nickel [29] and activation energy decreases with increasing a nickel content of the alloy. Table 4 shows specifications for chemical compositions of Hastelloy XR and X [30]. Though a kind of metal and its content by percentage of Hastelloy XR was similar to those of Hastelloy X, the corrosion resistance of Hastelloy XR was improved in high-temperature helium surroundings. However, we have no data regarding permeability of hydrogen and deuterium of Hastelloy XR, which is employed not only as a material of the heat transfer pipe of the IHX but also as one of candidate materials of the

Table 5. Main Specifications of Experimental Apparatus

Test section	: Coaxial double pipe and electric furnace
Permeation test pipe (inner)	: 24.8 mm I.D., 31.8 mm O.D. 3.5 mm thickness, 1000 mm length
Pipe material	: Hastelloy XR
Measuring pipe (outer)	: 50 mm I.D., 56 mm O.D. 3 mm thickness, 1000 mm length
Pipe material	: Hastelloy X
Working fluid	: Hydrogen, Deuterium, Helium, Argon, Nitrogen
Electric furnace	: Main heater 2 kW × 3 regions (vertical direction) Pre-heater 1 kW × 2 parts (supply and purge lines)
Maximum temperature	: 900 °C
Maximum pressure	: 1 MPa
Flow rate of gas	: 100 cc(STP)(*1)/min
Hydrogen measurement system	: Quadrupole mass spectrometer (*1)standard condition (0 °C, 0.1 MPa)

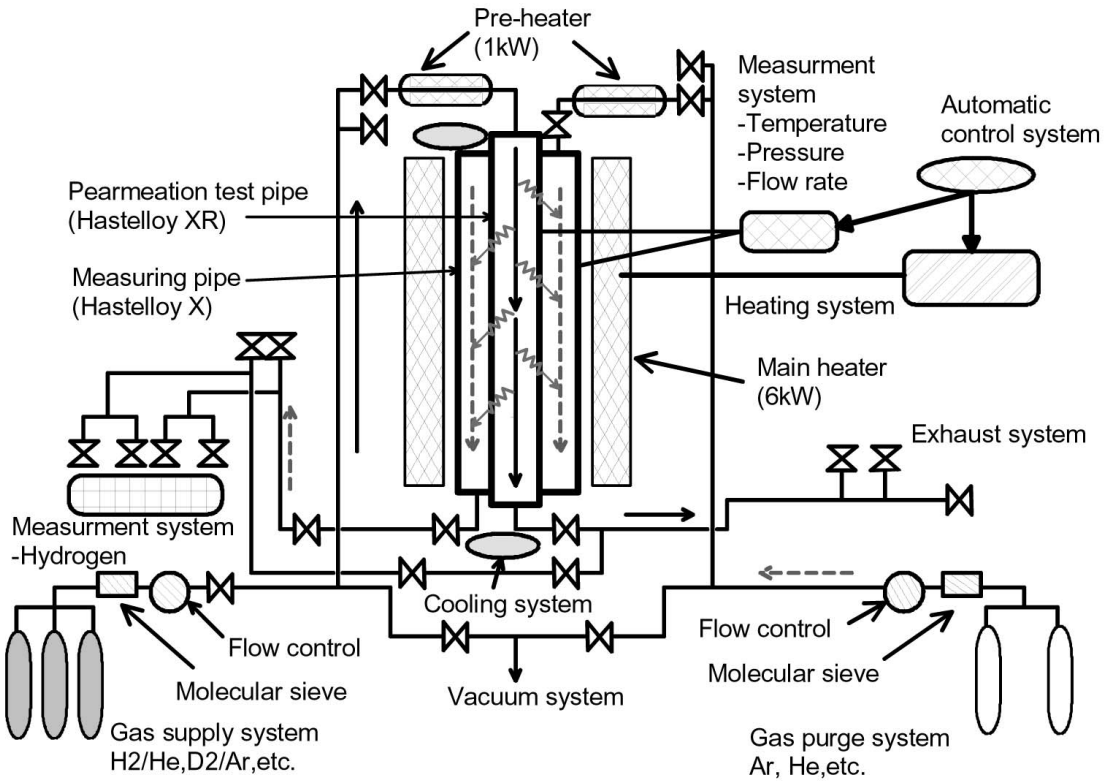

Fig. 16. Experimental Apparatus of Hydrogen Permeation

catalyst pipe of the SR. This paper describes permeability of hydrogen and deuterium of Hastelloy XR.

9.1.2 Experimental Apparatus and Procedure

An apparatus is composed of a test section which consists of a permeation test pipe (inside pipe), a measurement pipe (outside pipe), and an electric furnace, a gas supply system, a concentration measurement system, electric instruments, and so on. The partial pressure of hydrogen isotope is measured by a quadrupole mass spectrometer.

Table 6. Experimental Condition (Hydrogen Concentration and Temperature)

Gas	Partial pressure [Pa]	Concentration [ppm]	Temperature [℃]					
			600	650	700	750	800	850
H_2/He	3.95×10^3	3.95×10^4	H-1	H-2	H-3	H-4	H-5	H-6
	1.01×10^3	1.01×10^4	H-7	H-8	H-9	H-10	H-11	H-12
	1.06×10^2	1.06×10^3	-	-	H-13,14	H-15,16	H-17~22	H-23
	1.17×10	1.17×10^2	-	-	-	-	-	H-24
D_2/Ar	4.04×10^3	4.04×10^4	-	-	D-1	D-2	D-3	D-4
	9.89×10^2	9.89×10^3	-	-	D-5,6	D-7,8	D-9,10	D-11~13

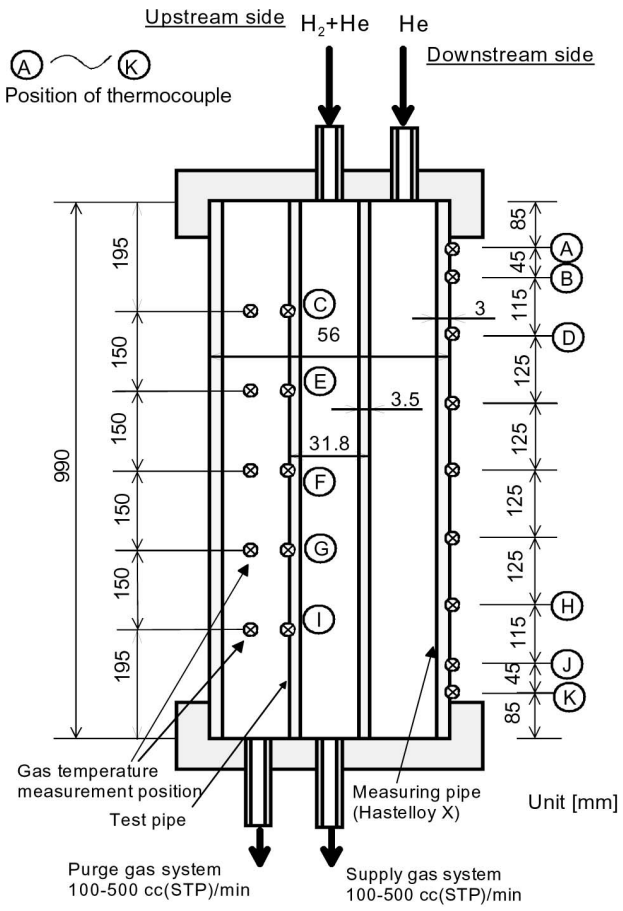

Fig. 17. Test Section of Apparatus and Measured Points of Wall and Gas Temperature

A schematic drawing of the experimental apparatus is provided in Fig. 16. Table 5 shows the main specification of the apparatus.

As for the condition of hydrogen partial pressure in this experiment, we have to maintain a constant hydrogen partial pressure in the permeation test pipe. This is because the gas mixture, which contains hydrogen isotope, flows steadily in the inside and outside of the heat transfer pipe of the IHX during a normal operation. Therefore, a test section was made a coaxial double pipe structure, which inserted the permeation test pipe into the measurement pipe, and gases flowed into the inside and outside of the permeation test pipe under the condition of constant pressure and flow rate. An inside pipe, which is the typical test pipe made of Hastelloy XR, has an inner diameter of 24.8 mm and a thickness of 3.5 mm as it is the same as the dimension of the heat transfer pipe of the IHX. In order to simulate the total pressure of the gas mixture up to 1 MPa, the measurement pipe was made of Hastelloy X whose hydrogen permeability is already known. The outside pipe has an inner diameter of 50 mm and a thickness of 3mm. The heating area of the electric furnace, which has 6 kW, is divided into three vertical regions in order to achieve a flat temperature distribution along the pipe. The each part was independently controlled and was heated up to 900ºC. A rough sketch of the test section can be seen in Fig. 17. The heating area between points D through H could be kept a flat temperature. However, the 250 mm regions from the both ends of the pipe were not achieved a flat temperature distribution. A partial pressure of permeated hydrogen decreases with increasing a gas flow rate in an annular passage between the permeation test pipe and the measurement pipe. So, a volumetric flow rate in the annular passage was decided from the result of a preliminary analysis [31]. The control range of the volumetric flow rate was made 0 ~ 1000 cc/min at 20ºC, 0.1 MPa. The partial pressure of hydrogen and deuterium was obtained by using a quadrupole mass spectrometer. Gas and water concentration can be measured to 1 ppm and 500 ppb, respectively, in this system. The exit of the gas supply, the permeation test pipe, and the annular passage was equipped with a concentration measuring tube. The wall and gas temperatures were measured with a K-type thermocouple.

The experimental procedure is as the following. At

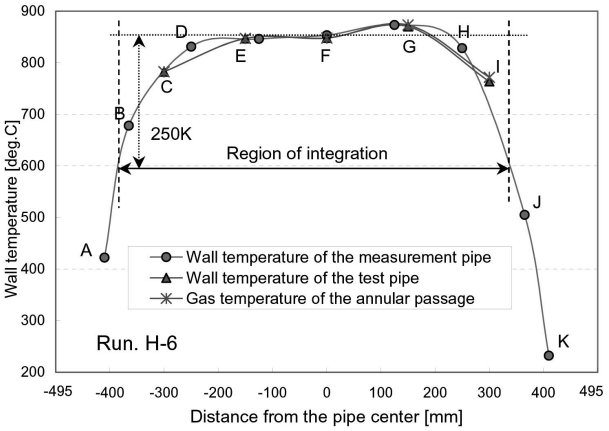

Fig. 18. Wall Temperature Distribution of the Test and Measurement Pipes (H-6)

first, the gas mixture containing hydrogen is supplied to the annular passage without heating and a coefficient of transformation to change hydrogen partial pressure into hydrogen concentration is obtained by measuring hydrogen partial pressure. Next, helium gas is flowed into the permeation test pipe and the annular passage when hydrogen permeation is examined; on the other hand, argon gas is flowed into there when deuterium permeation is examined. Total gas pressure in the test section was set to be 0.1 MPa. The test section is heated and maintained a constant temperature. If the temperature of the permeation test pipe becomes constant for more than 30 minutes, this condition was assumed to the steady state. Then, the gas mixture was supplied to the permeation test pipe. An experimental condition is shown in Table 6. The parameter of the experiment was made a wall temperature of the permeation test pipe, hydrogen and deuterium partial pressure. The flow rate of the supply and the purge gas was set at 100 cc(STP)/min and 500 cc(STP)/min, respectively. Here, (STP) means standard temperature (0ºC) and pressure (0.1 MPa) condition.

9.1.3 Experimental Results and Discussion

A preliminary experiment was performed to confirm molecular diffusion in the gas mixture would not become the rate-limiting step of the hydrogen transport process. The variation in flow rate have no influenced on the amount of permeated hydrogen. The variation in the amount of permeated hydrogen was within 5.3 % with flow rate ranging from 100 cc(STP)/min to 500 cc(STP)/min.

The longitudinal average temperature of the permeation test pipe can be obtained as following. The measured points of wall and gas temperatures in the test section are shown in Fig. 17. Figure 18 provides the wall and gas temperature distribution along the flow direction at the steady state condition. As shown in Fig. 17, the permeation test pipe, the measurement pipe, and the annular passage were equipped with 5, 9, and 5 thermocouples, respectively. As indicated in Fig. 18, it was found that wall temperature of the permeation test pipe (▲) and the measurement pipe (●), and the gas temperature (*) of the annular passage in the same vertical position are almost equal. Thus, an average temperature of the permeation test pipe was obtained by using temperature at 11 measured points (A~K) assuming that the wall temperature of the permeation test pipe equals to that of the measurement pipe. The wall temperature in the center of the permeation test pipe is maintained at about 850ºC. Hydrogen permeability of Hastelloy X in 600ºC decreases about 1/8 of the permeability in 850ºC and the surface area, which is less than 600ºC, is about 20 % of the whole area. Thus, the amount of permeated hydrogen through the pipe, which is less than 600ºC, is about 1 % of the one through the pipe, which is more than 600ºC. Therefore, the amount of permeated hydrogen from the low temperature part, which is lower than 250 K from the maximum temperature, was ignored. The average temperature of the permeation test pipe was calculated by the trapezoid formula.

The permeation flux J [m(STP)·s^{-1}] of hydrogen was obtained as follows. The relationship between hydrogen partial pressure in a gas phase and molar concentration of dissolved hydrogen on a surface of a pipe are assumed to obey Sieverts' law.

$$C_s = S\sqrt{p_{H2}} \tag{2}$$

Where, C_s is molar concentration of dissolved hydrogen. S [m^3(STP) · m^{-3} · Pa$^{-0.5}$] and p_{H2} [Pa] is solubility and hydrogen partial pressure, respectively.

The permeation flux can be written as the following equation.

$$J = -D_s\left(r/r_i\right)\left(dC_s/dr\right) \tag{3}$$

Where, r [m] is radius of a circular pipe and D_s [m^2 · s^{-1}] is a diffusivity of hydrogen in a solid metal.

Substitution of Eq. (2) into Eq. (3) and integration of Eq. (3) gives:

$$J = \frac{K_P}{r_i \cdot \ln\left(r_o/r_i\right)}\left(\sqrt{p_i} - \sqrt{p_o}\right). \tag{4}$$

Here, p_i and p_o [Pa] are hydrogen partial pressure in the permeation test pipe and the annular passage respectively; r_i and r_o [m] are an inner and an outer radius of the permeation test pipe. Hydrogen partial pressure in the permeation test pipe was assumed a constant in this experiment. It is assumed that hydrogen partial pressure at the inlet of the annular passage is zero. Hydrogen partial pressure at the outlet of the annular passage is obtained by the mass spectrometer. Then, hydrogen partial pressure, p_o, in the annular passage is assumed an arithmetic mean value of

hydrogen partial pressure at the inlet and outlet of the annular passage. K_P [m^3(STP)$\cdot m^{-1}\cdot s^{-1}\cdot Pa^{-0.5}$] is a permeability shown with the following equation.

$$K_P = D_s \cdot S = F_0 \exp(-E_0/RT) \quad (5)$$

Where, F_0 [m^3(STP)$\cdot m^{-1}\cdot s^{-1}\cdot Pa^{-0.5}$] and E_0 [$kJ\cdot mol^{-1}$] is a pre-exponential factor and an activation energy of hydrogen permeability. R [$J\cdot mol^{-1}\cdot K^{-1}$] is gas constant and T [K] is an absolute temperature of the pipe. An amount of permeated hydrogen Q [$m^3\cdot s^{-1}$] based on the inner radius of the permeation test pipe is shown by the following equation.

$$Q = 2\pi r_i l J = \frac{2\pi l K_{XR}}{\ln(r_o/r_i)}\left(\sqrt{p_i} - \sqrt{p_o}\right) \quad (6)$$

Where, l [m] is a pipe length and K_{XR} is the hydrogen permeability of Hastelloy XR.

The amount of permeated hydrogen, Q, was corrected by obtaining the amount of permeated hydrogen through the measurement pipe, Q_o.

$$Q_o = 2\pi r'_i L J_o = \frac{2\pi L K_X}{\ln(r'_o/r'_i)}\left(\sqrt{p_o} - \sqrt{p_a}\right) \quad (7)$$

Where, J_o is a permeation flux to the measurement pipe, K_X is the hydrogen permeability of Hastelloy X, p_o and p_a are hydrogen partial pressure in the annular passage and the outside of the measurement pipe. It is assumed p_a=0 because of the outside of the measurement pipe being the atmosphere. L is the pipe length; r'_i and r'_o is the inner and outer radius of the measurement pipe. Wall temperature of the measurement pipe is assumed to be equal to the one of the permeation test pipe, and the reported value is used for the hydrogen permeability of Hastelloy X. An effect on a decrease of the amount of permeated hydrogen by the oxide film will depend not only on a thickness but also on a state of formation of the oxide film. According to the reference [25], [32], the effectiveness factor for reduction of permeability by the oxide film is reported to be 1/100 ~ 1/1000. The oxide film was already formed on the outside surface of the measurement pipe because it was being heated at about 700°C under the atmospheric condition for more than 50 hours before the experiment started. From the results of the amount of supplied and permeated hydrogen through the test pipe in the preliminary experiment, it was confirmed that the amount of permeated hydrogen through the measurement pipe becomes less than 1/10 of the value calculated with Eq. (7). If the amount of permeated hydrogen through the measurement pipe is overestimated, the hydrogen isotope permeability will be evaluated conservatively. One-tenth of the value calculated by Eq. (7) was corresponding to 3.6% of the amount of permeated hydrogen obtained by the experiment. However, since the thickness of the oxide film increases with increasing the heated time, the amount of permeated hydrogen will decrease. Therefore, the amount of correction value decreases with increasing the heated time any further. Though it is expected that the correction value is lower than 1/10 of the value calculated by Eq. (7), the reduction factor by the oxide film will set to be 1/10 from the view point of conservative aspect. The accuracy of the measurment and the correction value decribed above were included in the error of the pre-exponential factor.

The sum of the amount of permeated hydrogen, Q_e, obtained by the experiment and the correction value, Q_o, is assumed to be equal to the total amount, Q, obtained by Eq. (6). Then, KXR becomes

$$K_{XR} = \frac{(Q_e + Q_o)\ln(r_o/r_i)}{2\pi l\left(\sqrt{p_i} - \sqrt{p_o}\right)}. \quad (8)$$

Hydrogen permeability obtained in this experiment is shown in Fig. 19, and the activation energy and the pre-exponential factor are shown in Table 7. A solid line shows the average value of hydrogen permeability obtained by three kinds of hydrogen partial pressures. A dotted line shows hydrogen permeability of Hastelloy X. The activation

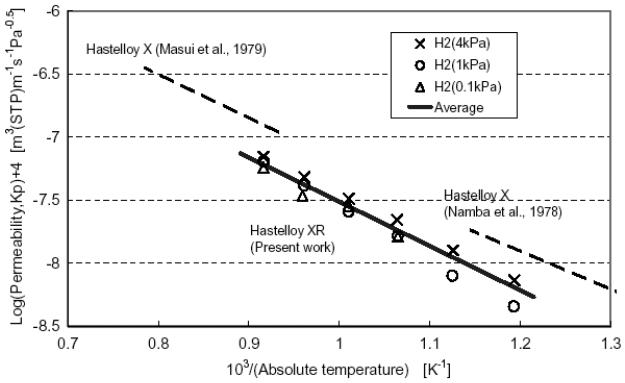

Fig. 19. Hydrogen Permeability of Hastelloy XR and Hastelloy X

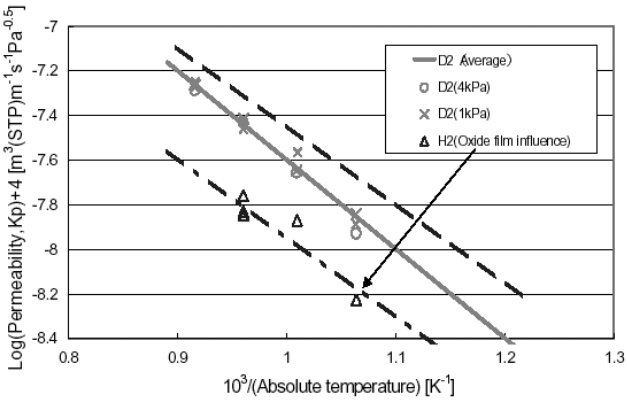

Fig. 20. Permeability of Hydrogen and Deuterium of Hastelloy XR

Table 7. Activation Energy and Pre-Exponential Factor of Permeability of H_2 and D_2

Gas species	Partial pressure [Pa]	Concentration [ppm]	Activation energy [kJ·mol^{-1}]	Pre-exponential factor [m^3(STP)·m^{-1}·s^{-1}·Pa$^{-0.5}$]
H_2	3.95×10^3	3.95×10^4	67.5	1.02×10^{-8}
H_2	1.01×10^3	1.01×10^4	68.1	1.01×10^{-8}
H_2	1.06×10^2	1.06×10^3	66.0	7.8×10^{-9}
H_2	Average		67.2±1.2	$(1.0\pm0.2)\times10^{-8}$
H_2*	1.06×10^2	1.06×10^3	70.2±2.0	$(4.7\pm0.4)\times10^{-9}$
D_2	4.04×10^3	4.04×10^4	76.1	2.31×10^{-8}
D_2	9.89×10^2	9.89×10^3	76.9	2.63×10^{-8}
D_2	Average		76.6±0.5	$(2.5\pm0.3)\times10^{-8}$

* : Some oxide film influence suspected.

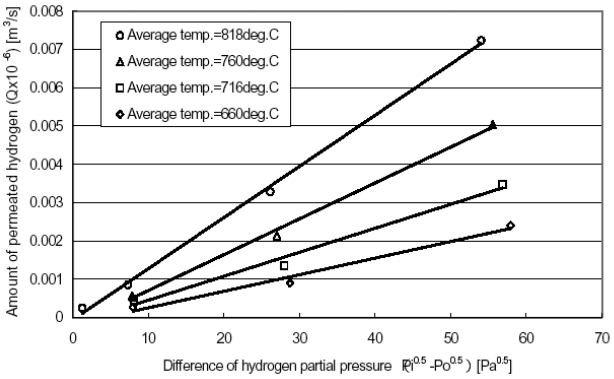

Fig. 21. Relationship Between Difference of Partial Pressure and Amount of Permeated Hydrogen

energy of hydrogen permeability of Hastelloy XR was almost equal to that of Hastelloy X.

Deuterium permeability of Hastelloy XR is shown in Fig. 20. How to calculate deuterium permeability is the same as the case of hydrogen permeability. According to the report [33], deuterium permeability becomes about $1/2^{0.5}$ times of hydrogen permeability. A dotted line in Fig. 20 shows hydrogen permeability at 3.95×10^3 Pa of hydrogen partial pressure. A solid line shows the approximate straight line obtained from deuterium permeability at 4.04×10^3 Pa (O) and 9.89×10^2 Pa ($\times$) of deuterium partial pressure by a least square method. Deuterium permeability obtained by the experiment is shown in Table 7.

High purity helium gas (99.9999%) and argon gas (99.995%) were used as a purge gas to prevent an oxidation of the pipe surface. Both of the supply and the purge gas system were equipped with a molecular sieve trap (MST). In order to examine an effectiveness of oxide film for the permeability, the permeation test pipe was heated at 600°C to 850°C during 140 hours under the condition of helium gas atmosphere and water concentration of less than 1ppm. Fig. 20 shows hydrogen permeability of Hastelloy XR with the oxide film. The symbol of triangle (D) indicates these experimental data and the dotted-dashed line shows the average value of them. The activation energy and pre-exponential factor with the oxide film are indicated in Table 7. The effectiveness factor for reduction of permeability is about 0.3 in the present experiment. It is confirmed that a high temperature part of the pipe was discolored and oxidized. It is expected that the amount of permeated tritium also reduce by the oxide film in the HTTR hydrogen production system because the oxide film will be formed on the surface of the IHX heat transfer pipe during the initial period of the reactor operation.

The amount of permeated hydrogen is in proportion to the difference in square root of hydrogen partial pressure as far as the rate-limiting step of the transport process is diffusion in the solid metal even if hydrogen partial pressure decreases. That is, if the rate-limiting step of permeation becomes diffusion in the solid metal, the molar concentration of dissolved hydrogen on a surface of the pipe will obey Sieverts' law. Therefore, it is expected that a straight line connecting experimental data pass through a zero point. Fig. 21 shows a dependence on partial pressure to the amount of permeated hydrogen. A horizontal axis shows the difference in square root of the partial pressure. The straight line connecting experimental data for each average temperature passes through the neighborhood of zero point. Therefore, the amount of permeated hydrogen will be in proportion to the difference in square root of the partial pressure as for the low partial pressure area as well.

10. CONCLUSIONS

JAEA is carrying out the R&D of HTGR safety technologies and the HTTR hydrogen production system. To establish the connecting technologies between a nuclear and a chemical plant, JAEA is designing the HTTR hydrogen production system. Prior to constructing the HTTR hydrogen production system, JAEA will perform the R&D of the safety and connecting technologies through the HTTR safety demonstration test, the out-of-pile test, and the component tests. The results will be reflected to design and licensing of the HTTR hydrogen production

system.

The present analysis and experiment were carried out to investigate the air ingress phenomena and to develop the passive safe technology for the prevention of air ingress and of graphite corrosion. On the other hand, experiment on hydrogen isotope permeation was performed to obtain permeability of hydrogen and deuterium of Hastelloy XR and to investigate the rate-limiting step of the process of hydrogen permeation phenomenon in the HTTR hydrogen production system. The following conclusions were obtained.

(1) There are two stages in the primary-pipe rupture accident of the HTTR. In the first stage of the accident, the molecular diffusion and the natural circulation of the gas mixture having the very slow velocity limit the air ingress rate. In the second stage of the accident, the ordinary natural circulation of air throughout the reactor limits the air ingress rate. Thus, the large amount of air flows into the reactor in the second stage of the accident.

(2) Three different states of air ingress phenomena existed in the present experiment, which depend on the cooling rate of the simulated core. In the first case, the temperature of the simulated core increased by the graphite oxidation reaction after the second stage started. In the second case, the temperature of the simulated core decreased by the natural circulation of air without graphite oxidation reaction. In the last state, the air ingress process terminated during the first stage of the accident and the ordinary natural circulation of air did not produced. Therefore, the safe cooling rate also exists in the HTTR as similar of this apparatus having the reverse U-shaped channel.

(3) A computer program has been developed to analyze thermal-hydraulic behavior during the first stage of the primary-pipe rupture accident of the HTGR. It has been found that the program is sufficiently versatile to analyze transient behavior during the accident. The program was validated with the simulation experiment. However, it is important to find the efficient computational algorithms, taking into account the use of vector or parallel computers, in order to get even faster computation. Transient calculations for the primary-pipe rupture accident require a time period spanning many hours or days.

(4) In the passive safe technology developing, the beginning of the ordinary natural circulation of air was prevented to inject helium gas into the low-temperature side of the pressure vessel. Thus, it is found that the helium injection method is useful for the prevention of air ingress in the future reactor. If the helium canister with small opening or crack can be made and installed into the pressure vessel, the onset of the ordinary natural circulation of air can be controlled passively. The passive safe study for the depressurization accident is underway.

(5) As hydrogen and deuterium permeability of Hastelloy XR were obtained for the first time, we can evaluate quantitatively the amount of permeated hydrogen isotope through the IHX prior to take the safety review for the construction of the HTTR hydrogen production system. Hydrogen and Deuterium permeability of Hastelloy XR is shown in Table 7.

(6) Hydrogen permeability of Hastelloy XR after about 140-hour heating under the less than 1 ppm water concentration was obtained. The effectiveness factor for reduction of permeability is about 0.3 in the present experiment. As it is expected that the oxidized film will be formed on the surface of the IHX heat transfer pipe, the amount of permeated hydrogen isotope through the pipes will be reduced in the HTTR hydrogen production system.

Nomenclature

A_e = flow area [m^2]
C = molar density [$mol \cdot m^{-3}$] or molar concentration [-]
c_p = specific heat capacity at constant pressure [$J \cdot g^{-1} \cdot K^{-1}$]
D_{i-m} = effective diffusion coefficient in the multi-component gas mixture [$m^2 \cdot s^{-1}$]
D_e = effective diameter of the stream-tube [m]
D : diffusion coefficient [$m^2 \cdot s^{-1}$]
d_i : inner diameter of pipe
d_t : thickness of pipe
E_0 : activation energy [kJ ·mol-1]
F_0 : pre-exponential factor [$m^3(STP) \cdot m^{-1} \cdot s^{-1} \cdot Pa^{-0.5}$]
f = friction factor [-]
g = acceleration of gravity [$m \cdot s^{-2}$]
J : steady-state permeation flux [$m \cdot s^{-1}$]
K_p: permeability [$m^3(STP) \cdot m^{-1} \cdot s^{-1} \cdot Pa^{-0.5}$]
L_h = length of heated periphery of the stream-tube. [m]
l, L : length of the test and measurement pipe [m]
M_m = molecular weight of the gas mixture [kg]
n = number of component gases [-]
p = fluid static pressure [Pa]
p_i : hydrogen partial pressure in the test pipe [Pa]
p_o : hydrogen partial pressure in the annular passege [Pa]
p_a: hydrogen partial pressure in the outside of the measurement pipe [Pa]
Q_i = production or dissipation term of the mass conservation equation [$m^3 \cdot s^{-1}$]
Q : amount of permeated hydrogen [$m^3 \cdot s^{-1}$]
Q_o: amount of permeated hydrogen through the measurement pipe [$m^3 \cdot s^{-1}$]
Q_e: amount of permeated hydrogen obtained by the experiment [$m^3 \cdot s^{-1}$]
R = gas constant [$J \cdot mol^{-1} \cdot K^{-1}$]
r, r': radius of test and measurement pipe [m]
S: solubility [$m^3(STP) \cdot m^{-3} \cdot Pa^{-0.5}$]
T = gas temperature [℃]
T_w = wall temperature [℃]
T: temperature [K]
u: velocity [$m \cdot s^{-1}$]
α = heat transfer coefficient [$J \cdot m^{-2} \cdot K^{-1}$]

β : ratio of permeability of hydrogen and deuterium [-]
λ : thermal conductivity [$W \cdot m^{-1} \cdot K$]
μ : viscosity [$kg \cdot m^{-1} \cdot s^{-1}$]
θ = inclination of flow direction [deg]
ρ : density [$kg \cdot m^{-3}$]
ω_i = mass fraction [-]
ξ : conversion ratio of methane [-]

Subscript

i : inner	o : outer
f : fluid phase	s : solid phase
H : hydrogen	D : deuterium
XR : Hastelloy XR	X : Hastelloy X

REFERENCES

[1] S. Saito, et al., "Design of High Temperature Engineering Test Reactor (HTTR)," JAERI-1332, Japan Atomic Energy Research Institute (1994).

[2] S. Shiozawa, et al., "Research and development of HTTR hydrogen production system in JAERI," *Proc. 12th Pacific Basin Nuclear Conference*, Seoul, Korea, **2**, 1007-1018 (2000).

[3] Y. Inagaki, et al., "Out-of-pile demonstration test of hydrogen production system coupling with HTTR," *Proc. 7th International Conference on Nuclear Engineering*, Tokyo, Japan, ICONE-7101, 1999.

[4] H. Ohashi, et al., "Performance test results of mock-up test facility of HTTR hydrogen production system," *Proc. 11th International Conference on Nuclear Engineering*, Tokyo, Japan, ICONE11-36059, 2003.

[5] T. Takeda, et al., "Study on tritium/hydrogen permeation in the HTTR hydrogen production system," *Proc. 7th International Conference on Nuclear Engineering*, Tokyo, Japan, ICONE-7102, 1999.

[6] H. Ohashi, et al., *Proc. 13th International Conference on Nuclear Engineering*, Beijing, China, May 16-20, ICONE13-50536, 2005.

[7] T. Takeda and M. Hishida, "Studies on diffusion and natural convection of two-component gases," *Nucl. Eng. Des*., **135**, 341-354 (1992).

[8] T. Takeda and M. Hishida, "Studies on molecular diffusion and natural convection in a multicomponent gas system," *Int. J. of Heat and Mass Transfer*, **39**, 527-536 (1996).

[9] M. Hishida, T. Takeda, and S. Takenaka, "Air ingress during the primary-pipe rupture accident of an HTGR," *Proc. 3rd JSME/ASME Joint International Conference on Nuclear Engineering*, Tokyo, Japan, **2**, 1093-1100, 1995.

[10] T. Takeda, et al., "Analysis of air ingress process during the primary-pipe rupture accident of the HTGR," *Proc. 3rd JAERI Symp. on HTGR Technologies*, JAERI-Conf 96-010, 275-288, 1996.

[11] T. Takeda and M. Hishida, "Study on the passive safe technology for the prevention of air ingress during the primary-pipe rupture accident of HTGR," *Nucl. Eng. Des*., **200**, 251-259 (2000).

[12] K. Kunitomi, et al., "Depressurization accident analysis for the HTTR by the TAC-NC," *Energy*, **16**, 471-480 (1991).

[13] K. Kunitomi, et al., "Thermal transient analyses during a depressurization accident in the HTTR," JAERI-M, 91-163 (1991), in Japanese.

[14] R. K. Shah and A. L. London, *Advances in Heat Transfer : Laminar Flow Forced Convection in Ducts*, p. 78, Academic, New York (1978).

[15] R. C. Reid, J. M. Prausnitz, and T. K. Sherwood, *The Properties of Gases and Liquids* **3rd Edn**., 37-40, 226, 410-414, 470-474, 548-565, McGraw-Hill, New York (1977).

[16] C. R. Wilke, "Diffusional properties of multicomponent gases," *Chem. Eng. Prog*., **46**, 95-104 (1950).

[17] D. F. Fairbanks and C. R. Wilke, "Diffusion coefficients in multicomonent gas mixture," *Ind. Eng. Chem*., **42**, 471-475 (1950).

[18] R. E. Walker, N. deHaas, and A. A. Westenberg, "Measurements of multicomponent diffusion coefficients for the CO2-He-N2 system using the point source technique," *J. Chem. Phys*., **32**, 1314-1316 (1960).

[19] S. V. Patankar, *Numerical Heat Transfer and Fluid Flow*, McGraw-Hill, New York (1980).

[20] D. B. Spalding, "A novel finite-difference formulation for differential expressions involving both first and second derivatives," *Int. J. Num. Methods Eng*., **4**, 551 (1972).

[21] K. Sawa, H. Mikami, and S. Saito, "Analytical method and results of off-site exposure during normal operation of high temperature engineering test reactor (HTTR)," *Energy*, **16**, 459-470 (1999).

[22] T. Takeda, J. Iwatsuki, and Y. Inagaki, "Permeability of hydrogen and deuterium of Hastelloy XR," *J. Nucl. Mater*., **326**, 47-58 (2004).

[23] T. Takeda and J. Iwatsuki, "Counter-permeation of deuterium and hydrogen through INCONEL600," *Nucl. Technol*., **146**, 83-95 (2004).

[24] R. A. Strehlow and H. C. Savage, "The permeation of hydrogen isotopes through structural metals at low pressures and through metals with oxide film barriers," *Nucl. Technol*., **22**, 127-137 (1974).

[25] H. D. Rohrig, et al., "Studies on the permeation of hydrogen and tritium in nuclear process heat installations," *Nucl. Eng. Des*., **34**, 157-167 (1975).

[26] Y. Mori and T. Nakada, BNES *Conf. on the HTR and Process Appl*., Inst. of Civil Eng., Westminster, London, Paper 49, 1974.

[27] K. Masui, H. Yoshida, and R. Watanabe, "Hydrogen permeation through Iron, Nickel, and heat resisting alloys at elevated temperatures," *Trans. ISIJ*, **19**, 547-552 (1979).

[28] T. Namba, et al., "Hydrogen permeation through Nickel and Hastelloy X," *J. Japan Inst. Metals*, **42**, 374-380 [in Japanese] (1978).

[29] W. M. Robertson, *Proc. International Meeting on Hydrogen in Metals*, Julich, Germany, **II**, 449 (1972).

[30] K. Hada, Y. Motoki, and O. Baba, Japan Atomic Energy Research Institute, JAERI-M 90-148 [in Japanese] (1990).

[31] T. Takeda, J. Iwatsuki, and T. Nishihara, "Study on hydrogen permeation through high-temperature tube in the HTTR heat utilization system," *Proc. 6th International Conference on Nuclear Engineering*, San Diego, CA, USA, ICONE-6125 (1998).

[32] W. A. Swansiger and R. Bastasz, "Tritium and deuterium permeation in stainless steels: Influence of thin oxide films," *J. of Nucl. Mater*. **85&86**, 335-339 (1979).

[33] H. Katsuta and K. Furukawa, "Hydrogen and deuterium transport through type 304 stainless steel at elevated temperatures," *J. of Nucl. Sci. and Technol*., **18**, 143-151 (1981).